

# Chapter 6

## Performance Characteristics of PET Scanners

### Introduction

In PET/CT and PET/MR imaging, PET images are of primary interest, whereas CT and MR images complement PET images by attenuation correction and fusion of images for better delineation of lesions. So we will discuss the performance parameters of only PET scanners. However, quality control tests for all three scanners are presented. A major goal of the PET studies is to obtain a good-quality and detailed image of an object by the PET scanner, and so it depends on how well the scanner performs in image formation. Several parameters associated with the scanner are critical to good-quality image formation, which include spatial resolution, sensitivity, noise, scattered radiations, and contrast. These parameters are interdependent, and if one parameter is improved, one or more of the others are compromised. A description of these parameters is given below.

### Spatial Resolution

The *spatial resolution* of a PET scanner is a measure of the ability of the device to faithfully reproduce the image of an object, thus clearly depicting the variations in the distribution of radioactivity in the object. It is empirically defined as the minimum distance between two points in an image that can be detected by a scanner. A number of factors discussed below contribute to the spatial resolution of a PET scanner.

*Detector size:* One factor that greatly affects the spatial resolution is the intrinsic resolution of the scintillation detectors used in the PET scanner. For multidetector PET scanners, the intrinsic resolution ( $R_i$ ) is related to the detector size  $d$ .  $R_i$  is normally given by  $d/2$  on the scanner axis at midposition between the two detectors and by  $d$  at the face of either detector (Fig. 6.1). Thus, it is best at the center of the

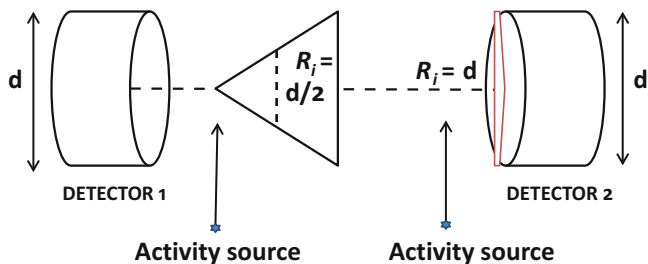


**Fig. 6.1** Illustration of spatial resolution  $R_i$  of a PET camera, the detector size of which is  $d$ . The  $R_i$  at any position along the LOR between the two detectors is given by the full width at half maximum (FWHM) of the activity distribution profile obtained by counting a point source of activity across the detector face at the position. The  $R_i$  is  $d/2$  at the center of the FOV determined by the FWHM from a triangular profile, while it is  $d$  at the edge of the FOV (i.e., the face of the detector) indicated by the red-lined near-rectangular box

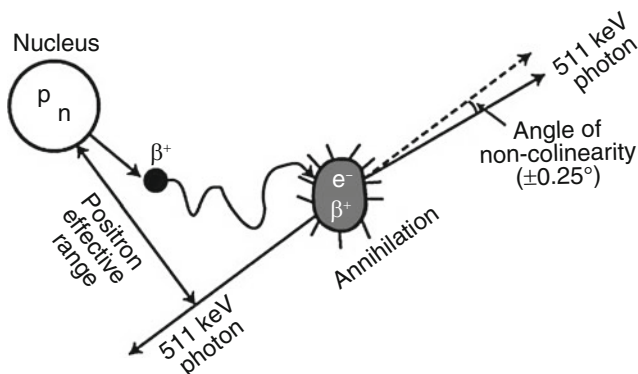


**Fig. 6.2** Positrons travel a distance before annihilation in the absorber and the distance increases with positron energy. Since positrons with different energies travel in zigzag directions, the effective range is the shortest distance between the nucleus and the direction of 511-keV photons. This effective range degrades the spatial resolution of the PET scanner (Reprinted with the permission of the Cleveland Clinic Center for Medical Art and Photography ©2009. All rights reserved)

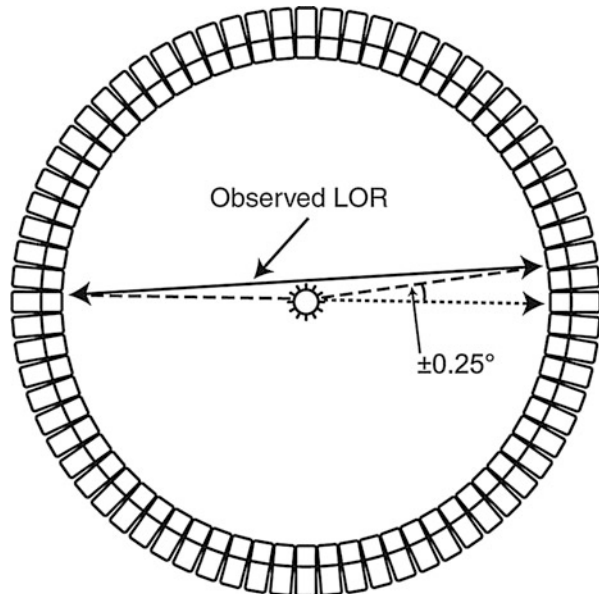
FOV and deteriorates toward the edge of the FOV. For a 6-mm detector, the  $R_i$  value is  $\sim 3$  mm at the center of the FOV and  $\sim 6$  mm toward the edge of the FOV. For continuous single detectors, however, the intrinsic resolution depends on the number of photons detected, not on the size of the detector, and is determined by the full width at half maximum (FWHM) of the photopeak.

*Positron range:* A positron with energy travels a distance in tissue, losing most of its energy by interaction with atomic electrons and then is annihilated after capturing an electron (Fig. 6.2). Thus, the site of  $\beta^+$  emission differs from the site of annihilation as shown in Fig. 6.2. The distance (range) traveled by the positron increases with its energy but decreases with the tissue density.

Since the positrons are deflected after interaction with electrons resulting in a zigzag trajectory, the positron range is essentially an effective range, which is given by the shortest (perpendicular) distance from the emitting nucleus to the positron annihilation line. Furthermore, positrons are emitted with a distribution of energy, which also affects the effective range. The effective positron ranges in water for  $^{18}\text{F}$  ( $E_{\beta^+, \text{max}} = 0.64 \text{ MeV}$ ) and  $^{82}\text{Rb}$  ( $E_{\beta^+, \text{max}} = 3.35 \text{ MeV}$ ) are 2.2 and 15.5 mm, respectively (Table 1.2). Since coincidence detection is related to the location of annihilation and not to the location of  $\beta^+$  emission, an error ( $R_p$ ) occurs in the localization of true position of the positron emission thus resulting in the degradation of spatial resolution. This contribution ( $R_p$ ) to the overall spatial resolution is determined from the FWHM of the positron count distribution, which turns out to be 0.2 and 2.6 mm for  $^{18}\text{F}$  and  $^{82}\text{Rb}$ , respectively (Tarantola et al. 2003).

*Noncolinearity:* Another factor of concern is the noncolinearity that arises from the deviation of the two annihilation photons from the exact  $180^\circ$  position. That is, two 511-keV photons are not emitted at exactly  $180^\circ$  after the annihilation process (Fig. 6.3), because of some small residual momentum of the positron at the end of the positron range. The maximum deviation from the  $180^\circ$  direction is  $\pm 0.25^\circ$  (i.e.,  $0.5^\circ$  FWHM). Thus, the observed LOR between the two detectors does not intersect the point of annihilation, but is somewhat displaced from it, as illustrated in Fig. 6.3. This error ( $R_a$ ) degrades the spatial resolution of the scanner and deteriorates with the distance between the two detectors. If  $D$  is the distance in cm between the two detectors (i.e., detector ring diameter), then  $R_a$  can be calculated from the point-spread function (PSF) as follows:

**Fig. 6.3** Noncolinearity of 511-keV annihilation photons. Because there is some residual momentum associated with the positron, the two annihilation photons are not emitted exactly at  $180^\circ$  but at a slight deviation from  $180^\circ$ . Two detectors detect these photons in a straight line, which is slightly deviated from the original annihilation line. The maximum deviation is  $\pm 0.25^\circ$  (Reprinted with the permission of the Cleveland Clinic Center for Medical Art and Photography ©2009. All rights reserved)



$$R_a = 0.0022D. \quad (6.1)$$

The contribution from noncolinearity worsens with larger diameter of the ring, and it amounts to 1.8–2 mm for currently available 80–90-cm PET scanners.

*Reconstruction method used:* Choice of filters with a selected cutoff frequency in the filtered backprojection reconstruction method may introduce additional degradation of the spatial resolution of the scanner. For example, a filter with a too high cutoff value introduces noise and thus degrades spatial resolution. An error ( $K_r$ ) due to the reconstruction technique is usually a factor of 1.2–1.5 depending on the method (Huesman 1977).

*Localization of detector:* The use of block detectors instead of single detectors causes an error ( $R_\ell$ ) in the localization of the detector by  $X, Y$  analysis and it may amount to 2.2 mm for BGO detectors (Moses and Derenzo 1993). However, it can be considerably minimized by using better light output scintillators, such as LSO.

Combining the above factors, the overall spatial resolution  $R_t$  of a PET scanner is given by

$$R_t = K_r \times \sqrt{R_i^2 + R_p^2 + R_a^2 + R_\ell^2}. \quad (6.2)$$

In whole-body scanners, the detector elements are normally large, and therefore,  $R_i(d$  or  $d/2)$  is large so that the contribution of  $R_p$  is negligible for  $^{18}\text{F}$ -FDG ( $E_{\beta^+, \max} = 0.64 \text{ MeV}$ ) whole-body imaging. For  $^{18}\text{F}$ -FDG studies using a 90-cm diameter PET scanner with 6-mm detectors,  $R_a \sim 2$  mm, and assuming  $R_p = 0$ ,  $R_\ell = 2.2$  mm, and  $K_r = 1.5$ ,  $R_t = 1.5 \times \sqrt{3^2 + (2.2)^2 + 2^2} = 6.3$  mm at the center of FOV and  $R_t = 1.5 \times \sqrt{6^2 + (2.2)^2 + 2^2} = 10.0$  mm at the edge of FOV of the scanner. However, the contribution of  $R_p$  may be appreciable for high-energy positron emitters (e.g.,  $^{82}\text{Rb}$ ;  $E_{\beta^+, \max} = 3.35 \text{ MeV}$ ) and small-animal PET scanners (e.g., microPET system) having smaller detectors.

The detailed method of measuring the spatial resolution of a PET scanner is given later in this chapter. The spatial resolutions of PET scanners from different manufacturers are given in Table 6.1.

## Sensitivity

The sensitivity of a PET scanner is defined as the number of counts per unit time detected by the device for each unit of activity present in a source. It is normally expressed in counts per second per microcurie (or kilobecquerel) (cps/ $\mu\text{Ci}$  or cps/kBq). Sensitivity depends on the geometric efficiency, detection efficiency,

**Table 6.1** Performance data of different PET scanners

Manufacturers→ <sup>a</sup> Models→	Philips <sup>b</sup>		Siemens <sup>c</sup>		GE <sup>c</sup>	
	GEMINI TF	GEMINI TF	Biograph	Biograph	Discovery	Discovery
Features↓	Big Bore	64 (PET/CT)	mCT	TruePoint	VCT	PET/CT 600
Sensitivity – 3D (cps/kBq/cc)	7.2	7.2	9.5	7.6	9.1	9.1
Transverse Resol. at 1 cm (mm)	4.7	4.7	4.4	4.2	5.0 (2D) 5.0 (3D)	5.1
Transverse Resol. at 10 cm (mm)	5.2	5.2	5.8	4.8	5.4 (2D) 5.4 (3D)	5.6
Axial resol. at 1 cm (mm)	4.7	4.7	4.5		5.0 (2D) 5.0 (3D)	5.6
Axial resol. at 10 cm (mm)	5.2	5.2	4.8	5.5	5.6 (3D)	6.3
Peak noise Equivalent Count rate (kcps) (3D)	94	110	100	165 170 (TrueV)	78	76
Scatter fraction (%)	31	30	<36	<36	36	38

<sup>a</sup>Reprinted with permission, Copyright 2009, ECRI institute, <http://www.ecri.org>, 5200 Butler Pike, Plymouth Meeting, PA 19462. 610-825-6000

<sup>b</sup>Data supplied by Philips Healthcare, USA

<sup>c</sup>Reprinted with permission, Copyright 2009, Imaging Technology News (<http://www.itonline.net>), Scranton Gillette Communications (<http://www.scrantongillette.com>) 3030 W. Salt Creek Lane, Suite 201, Arlington Heights, IL 60005-5025. Some of Siemens data were provided by Annemarie Grammens, Siemens Medical Solutions, USA

PHA window settings, and dead time of the system. The detection efficiency of a detector depends on the scintillation decay time, density, atomic number, and thickness of the detector material that have been discussed in Chap. 2. Also, the effect of PHA window setting on detection efficiency has been discussed in Chap. 2. The effect of the dead time on detection efficiency has been described in Chap. 3. In the section below, only the effects of geometric efficiency and other related factors will be discussed.

The geometric efficiency of a PET scanner is defined by the solid angle projected by the source of activity at the detector. The geometric factor depends on the distance between the source and the detector, the diameter of the ring, and the number of detectors in the ring. Increasing the distance between the detector and the source reduces the solid angle and thus decreases the geometric efficiency of the scanner and vice versa. Increasing the diameter of the ring decreases the solid angle subtended by the source at the detector, thus reducing the geometric efficiency and in turn the sensitivity. Also the sensitivity increases with increasing number of rings in the scanner.

Based on the above factors discussed, the sensitivity  $S$  of a single-ring PET scanner can be expressed as (Budinger 1998)

$$S = \frac{A \cdot \varepsilon^2 \cdot e^{-\mu t} \cdot 3.7 \times 10^4}{4\pi r^2} (\text{cps}/\mu\text{Ci}), \quad (6.3)$$

where  $A$  = detector area seen by a point source to be imaged,  $\varepsilon$  = detector's efficiency,  $\mu$  is the linear attenuation coefficient of 511-keV photons in the detector material,  $t$  is the thickness of the detector, and  $r$  is the radius of the detector ring. The proportionality to  $\varepsilon^2$  arises from the two detectors with efficiency  $\varepsilon$ , i.e.,  $\varepsilon \times \varepsilon$ . So if the single-detector efficiency is reduced by half, the coincidence detection efficiency is  $\varepsilon/2 \times \varepsilon/2 = \varepsilon^2/4$ .

Equation (6.3) is valid for a point source at the center of a single-ring scanner. For an extended source at the center of such scanners, it has been shown that the geometric efficiency is approximated as  $w/2r$ , where  $w$  is the axial width of the detector element and  $r$  is the radius of the ring (Cherry et al. 2003). Thus, the sensitivity of a scanner is highest at the center of the axial FOV and gradually decreases toward the periphery. In typical PET scanners, there are also multiple rings and each detector is connected in coincidence with as many as half the number of detectors on the opposite side in the same ring as well as with detectors in other rings. Thus, the sensitivity of multiring scanners will increase with the number of rings.

Note that the sensitivity of a PET scanner increases as the square of the detector efficiency, which depends on the scintillation decay time and stopping power of the detector. This is why LSO, LYSO, and GSO detectors are preferred to NaI(Tl) or BGO detectors (see Table 2.1). In 2D acquisitions, system sensitivity is compromised because of the use of septa between detector rings, whereas these septa are retracted or absent in 3D acquisition, and hence the sensitivity is increased by a factor of 4–8. However, in 3D mode, random and scatter coincidences increase significantly, the scatter fraction being 30–40% compared to 15–20% in 2D mode. The overall sensitivities of PET scanners for a small-volume source of activity are about 0.2–0.5% for 2D acquisition and about 2–10% for 3D acquisition, compared to 0.01–0.03% for SPECT studies (Cherry et al. 2003). The greater sensitivity of the PET scanner results from the absence of collimators in data acquisition.

Sensitivity is given by volume sensitivity expressed in units of  $\text{kcps}/\mu\text{Ci}/\text{cc}$  or  $\text{cps}/\text{Bq}/\text{cc}$ . It is determined by acquiring data in all projections for a given duration from a volume of activity (uniformly mixed) and dividing the total counts by the duration of counting and the concentration of the activity in the source. Manufacturers normally use this unit as a specification for the PET scanners. The detailed method of determining volume sensitivity is described under acceptance tests in this chapter. The volume sensitivities of PET scanners from different manufacturers are given in Table 6.1.

## Noise Equivalent Count Rate

Image noise is the random variation in pixel counts across the image and is given by  $(1/\sqrt{N}) \times 100$ , where  $N$  is the counts in the pixel. It can be reduced by increasing the total counts in the image. More counts can be obtained by imaging for a longer period, injecting more radiopharmaceutical, or improving the detection efficiency of the scanner. All these factors are limited by various conditions, e.g., too much activity cannot be administered because of increased radiation dose to the patient, random coincidence counts, and dead-time loss. Imaging for a longer period may be uncomfortable to the patient and improving the detection efficiency may be limited by the design of the imaging device.

The image noise is characterized by a parameter called the noise equivalent count rate (NECR) which is given by

$$\text{NECR} = \frac{T^2}{T + S + R}, \quad (6.4)$$

where  $T$ ,  $R$ , and  $S$  are the true, random, and scatter coincidence count rates, respectively. This value is obtained by using a 20-cm cylindrical phantom of uniform activity placed at the center of the FOV and measuring prompt coincidence counts. Scatter and random events are measured according to methods described later in this chapter. The true events ( $T$ ) are determined by subtracting scatter ( $S$ ) and random ( $R$ ) events from the prompt events. From the knowledge of  $T$ ,  $R$ , and  $S$ , the NECR is calculated by Eq. (6.4). The NECR is proportional to the signal-to-noise (SNR) ratio in the final reconstructed images and, therefore, serves as a good parameter to compare the performances of different PET scanners. The 3D method has a higher NECR at low activity. However, the peak NECR in the 2D mode is higher than the peak NECR in the 3D mode at higher activity. Image noise can be minimized by maximizing NECR.

Another type of image noise arises from nonrandom or systematic addition of counts due to imaging devices or procedural artifacts. For example, bladder uptake of  $^{18}\text{F}$ -FDG may obscure the lesions in the pelvic area. Various “streak”-type artifacts introduced during reconstruction may be present as noise in the image.

## Scatter Fraction

The scatter fraction (SF) is another parameter that is often used to compare the performances of different PET scanners. It is given by

$$SF = \frac{C_s}{C_p}, \quad (6.5)$$

where  $C_s$  and  $C_p$  are the scattered and prompt count rates. The lower the SF value, the better the performance of a scanner and better the quality of images. The method of determining SF is given later in this chapter. Comparative SF values for different PET scanners are given in Table 6.1.

## Contrast

Contrast of an image arises from the relative variations in count densities between adjacent areas in the image of an object. Contrast ( $C$ ) gives a measure of the detectability of an abnormality relative to normal tissue and is expressed as

$$C = \frac{A - B}{A}, \quad (6.6)$$

where  $A$  and  $B$  are the count densities recorded in the normal and abnormal tissues, respectively.

Several factors affect the contrast of an image, namely, count density, scattered radiations, type of film, size of the lesion, and patient motion. Each contributes to the contrast to a varying degree. These factors are briefly discussed here.

Statistical variations of the count rates give rise to noise that increases with decreasing information density or count density (counts/cm<sup>2</sup>) and are given by  $(1/\sqrt{N}) \times 100$ , where  $N$  is the count density. For a given image, a minimum number of counts are needed for a reasonable image contrast. Even with adequate spatial resolution of the scanner, lack of sufficient counts may give rise to poor contrast due to increased noise, so much so that lesions may be missed. This count density in a given tissue depends on the administered dosage of the radiopharmaceutical, uptake by the tissue, length of scanning, and detection efficiency of the scanner. The activity of a dosage, scanning for a longer period, and the efficiency of a scanner are optimally limited, as discussed above under NECR. The uptake of the tracer depends on the pathophysiology of the tissue in question. Optimum values for a procedure are obtained from the compromise of these factors.

Scattered radiations increase the background in the image and thus degrade the image contrast. Maximum scatter radiations arise from the patient. Narrow PHA window settings can reduce the scatter radiations, but at the same time the counting efficiency is reduced.

Image contrast to delineate a lesion depends on its size relative to system resolution and its surrounding background. Unless a minimum size of a lesion



develops larger than system resolution, contrast may not be sufficient to appreciate the lesion, even at higher count density. The effect of lesion size depends on the background activity surrounding it and on whether it is a “cold” or “hot” lesion. A relatively small-size “hot” lesion is easily well contrasted against a lower background, whereas a small-size “cold” lesion may be missed against the surrounding background of increased activities.

Film contrast is a component of overall image contrast and depends on the type of film used. The density response characteristics of X-ray films are superior to those of Polaroid films and provide the greatest film contrast, thus adding to the overall contrast. Developing and processing of exposed films may add artifacts to the image and, therefore, should be carried out carefully.

Patient motion during imaging reduces the image contrast. This primarily results from the overlapping of normal and abnormal areas due to movement of the organ. It is partly alleviated by restraining the patient or by having the patient in a comfortable position. Artifacts due to heart motion can be reduced by using the gated technique. Similarly, breath holding may improve the thoracic images.

## Quality Control of PET Scanner

In the image formation of an object using PET scanners, several parameters related to the scanners play a very important role. To ensure high quality of images, several quality control tests must be performed routinely on the scanner. The frequency of these tests is either daily or weekly or even at a longer interval depending on the type of parameter to be evaluated.

### *Daily Quality Control Tests*

*Sinogram (uniformity) check:* Sinograms are obtained daily using a long-lived  $^{68}\text{Ge}$  or  $^{137}\text{Cs}$  source mounted by brackets on the gantry and rotating it around the scan field without any object in the scanner. It can also be done by using a standard phantom containing a positron emitter at the center of the scanner. All detectors are uniformly exposed to radiations to produce homogeneous detector response and hence a uniform sinogram. A malfunctioning detector pair will appear as a streak in the sinogram.

Typically, the daily acquired blank sinogram is compared with a reference blank sinogram obtained during the last setup of the scanner. The difference between the two sinograms is characterized by the value of the so-called average variance, which is a sensitive indicator of various detector problems. It is expressed by the square sum of the differences of the relative crystal efficiencies between the two scans weighted by the inverse variances of the differences. The sum divided by the total number of crystals is the average variance. It is essentially an  $\chi^2$  value. If the

average variance exceeds 2.5, recalibration of the PET scanner is recommended, whereas for values higher than 5.0, the manufacturer's service is warranted (Buchert et al. 1999). In Fig. 3.4, the average variance between the two scans is 1.1, indicating all detectors are working properly.

### ***Weekly Quality Control Tests***

In the weekly protocol, system calibration and plane efficiency are performed by using a uniform standard phantom filled with radioactivity, and normalization is carried out by using a long-lived radionuclide rotating around the field of view or a standard phantom with radioactivity placed at the center of the scanner.

*System calibration:* A system calibration scan is obtained by placing the standard phantom containing a positron emitter in a phantom holder at the center of the FOV for uniform attenuation and exposure. The reconstructed images are checked for any nonuniformity. A bad detector indicates a decreased activity in the image and warrants the adjustment of PM tube voltage and the discriminator settings of PHA.

*Normalization:* As discussed in Chap. 3, normalization corrects for nonuniformities in images due to variations in the gain of PM tubes, the location of the detector in the block, and the physical variation of the detector. This test is carried out by using a rotating rod source of a long-lived radionuclide (normally  $^{68}\text{Ge}$ ) mounted on the gantry parallel to the axis of the scanner or using a standard phantom containing a positron emitter at the center of the scanner. The activity used in the source is usually low to avoid dead-time loss. Data are acquired in the absence of any object in the FOV. The source activity exposes all detectors uniformly. The multiplication factor for each detector is calculated by dividing the average of counts of all detector pairs by each individual detector pair count (i.e., along the LOR) Eq. (3.3). These factors are saved and later applied to the corresponding detector pairs in the acquired emission data of the patient Eq. (3.4). Normalization factors normally are determined weekly or monthly. To have better statistical accuracy in individual detector pair counts, several hours of counting is necessary depending on the type of scanner, and therefore, overnight acquisition of data is often made.

*Dose calibration of PET scanner:* Standard uptake values (SUV) and other parameters of PET images are often calculated that require the knowledge of absolute activity in regions of interest (ROI). The counts (corrected for randoms, dead time, scatter, and attenuation) in individual pixels of the ROI are converted to absolute activity by using calibration factors. To calculate the calibration factor,  $CF$ , a cylindrical phantom (normally 20 cm long and 20 cm in diameter) containing a known amount of positron-emitter activity (e.g.,  $^{68}\text{Ge}$  or  $^{18}\text{F}$ ) in a known volume is scanned, and an image is obtained. The calculated concentration of activity ( $A_{\text{cal}}$ ) is given by

$$A_{\text{cal}} = \frac{A}{V} \times N \times \exp[-0.693t/t_{1/2}], \quad (6.7)$$

where  $A$  is the activity (Bq or  $\mu\text{Ci}$ ) in the phantom measured in a dose calibrator,  $V$  is the volume of the phantom (mL),  $N$  is the branching ratio of positron decay of the radionuclide,  $t$  is the time delay from initial measurement to the start of the scan, and  $t_{1/2}$  is the half-life of the radionuclide used. Some investigators determine the activity by measuring an aliquot of the sample in a well counter whose counting efficiency is known.

Images are reconstructed using the scan data of the phantom after correction for scatter, randoms, and attenuation. Using a large ROI on each of the central image slices, the mean ROI activity (Bq/pixel or  $\mu\text{Ci}/\text{pixel}$ ) for each slice is calculated, from which an average measured activity  $A_{\text{measured}}$  is calculated using the ROIs of all slices. The calibration factor  $CF$  is then given by

$$CF = \frac{A_{\text{measured}}}{A_{\text{cal}}}. \quad (6.8)$$

$CF$  is applied to the measured activity in each voxel of the ROI of interest of the patient scan (by dividing) to calculate the absolute activity, which is then multiplied by the area of the ROI to obtain SUV. Note that if the radionuclide in the patient study is different from the calibration source radionuclide, the branching ratio  $N$  of the radionuclide must be taken into calculation. This calibration of PET scanners should be performed at installation, after major service or at least annually.

## Quality Control of CT Scanner

Like PET scanners, CT scanners need daily QC testing to check if they are performing within acceptable limits of operational parameters. Most of the daily tests are automatic and less rigorous. These tests include tube voltage, mA setting, and detector response, which are available as system-ready messages. Operator-based daily QC tests include the evaluation of image uniformity, accuracy of CT numbers of water (given in Hounsfield unit HU), tube voltage, and image noise measured at commonly used voltages. The uniformity is assessed by observing the display of a CT image of a phantom. Water CT numbers and standard deviations are measured by using a water phantom in the scan plane and should be within  $0 \pm 5$  HU. All these measurements are mostly menu driven initiated by the manufacturers' software, and the final result is often given in the form of PASS/FAIL display. Other parameters such as slice thickness, spatial resolution, contrast resolution, linearity, and laser alignment are assessed monthly or quarterly as recommended by the manufacturers.

An important parameter, CT dose index (*CTDI*, defined as the cumulative dose along the patient's axis for a single tomographic image), should be evaluated at least semiannually at different values of kVp and mA. It is measured by using an ionization chamber or thermoluminescent dosimeters placed in a tissue-equivalent acrylic phantom simulating the head or body. ACR (2015)<sup>1</sup> recommends reference doses (*CTDI*) of 7.5 mrad (75 mGy) for adult head, 2.5 rad (25 mGy) for adult abdomen and 3.5 rad (35 mGy) for pediatric (1-yr old) head. The details of these measurements are available in standard CT physics books.

## Quality Control of MR Scanner

The American College of Radiology (ACR) mandates that like other imaging devices, quality control (QC) tests are performed on MR scanners to obtain better images of patients, especially for accreditation of an institution. In order to perform these tests, the ACR has introduced short cylindrical phantoms made of acrylic plastic with specific dimensions, which are called ACR phantoms and has two sizes—small and large. Inside the phantoms, there are several complex structures to generate suitable images for quantitative or qualitative analysis. Specifications and frequencies of the tests to be performed are given by the ACR. Some tests are performed daily and some others weekly or annually. The common routine QC tests for optimum operation of MR scanners are listed below:

1. *Geometric efficiency*: It measures the lengths on the images between locations in the phantom and compares them with the true values of those lengths. Affected by miscalibrated gradient and inhomogeneity in magnetic field (daily or weekly).
2. *High-contrast spatial resolution*: It is a measure of how well the MR scanner can delineate the structures on the images and determined by the spatial resolution of the holes inside the phantom. It is specific but not sensitive and also affected by the poor gradient and inhomogeneity in magnetic field (daily or weekly).
3. *Uniformity*: It indicates the constant signal response throughout the image obtained of the phantom filled with water. It is calculated in percent from the high and low signals from an ROI on the phantom image as  $\% = [(1 - (\text{high} - \text{low}) / (\text{high} + \text{low}))]$ .
4. *Slice thickness*: The accuracy of slice thickness is assessed by comparing the measured and assigned slice thicknesses (annually).

---

<sup>1</sup> Data used with permission of the American College of Radiology (ACR). No other representation of this material is authorized without expressed, written permission from the ACR. Refer to the ACR website at [www.acr.org](http://www.acr.org) (Computed Tomography Accreditation) for the most current and complete information.

5. *Slice position accuracy*: It is measured by the difference between the assigned and actual positions of specific sites using 45° cross wedges in the ACR phantom, which appear as bars on the image (annually).
6. *Percent signal ghosting*: These are artifacts caused by a faint copy (ghost) of the imaged object appearing superimposed on the image, displaced from its true location, and essentially result from signal instability between pulse cycle repetitions.
7. *Low-contrast detectability*: This test assesses how low-contrast objects are delineable in the image obtained by using the ACR phantom that contains a set of low-contrast objects of various sizes and contrast. The low-contrast detectability is determined by contrast-to-noise ratios in the image and is affected by artifacts like ghosting.

For most tests the ACR phantom filled with water solution of various paramagnetic ions such as manganese, copper, and nickel is used and positioned at the center of the magnet. Scanning is performed for all tests with preset scan parameters such as pulse sequence, timing parameters (T1, T2, TR, TE, etc.), flip angle, matrix size, field of view, RF power setting, slice thickness, number of acquisition, and other relevant parameters. Some tests can be performed by technologists, whereas others must be performed by certified medical physicists, as required by the ACR. The details of these tests are available from [acr.org](http://acr.org) and also the American Association of Physicists in Medicine (AAPM 2010).

## Acceptance Tests for PET Scanner

Acceptance tests are a battery of quality control tests performed to verify various parameters specified by the manufacturer for a PET scanner. These are essentially carried out soon after a PET scanner is installed in order to establish the compliance of specifications of the device. The most common and important specifications are transverse radial, transverse tangential, and axial resolutions; sensitivity; scatter fraction; and count rate performance. It is essential to have a standard for performing these tests so that a meaningful comparison of scanners from different manufacturers can be made.

In 1991, the Society of Nuclear Medicine (SNM) established a set of standards for these tests for PET scanners (Karp et al. 1991). Afterward, in 1994, the National Electrical Manufacturers Association (NEMA) published a document, NU 2-1994, recommending improved standards for performing these tests, using a 20 × 19-cm phantom (NEMA 1994) (Fig. 6.4a). This phantom was useful for earlier scanners, in which the FOV was less than 17 cm and data were acquired in 2D mode, because of the use of septa. Modern whole-body PET scanners have FOVs as large as 25 cm and employ 3D data acquisition in the absence of septa. The coincidence gamma cameras have typical FOVs of 30–40 cm. Because of larger FOVs and high count rates in 3D mode, the NU 2-1994 phantom may not be accurately applied for some

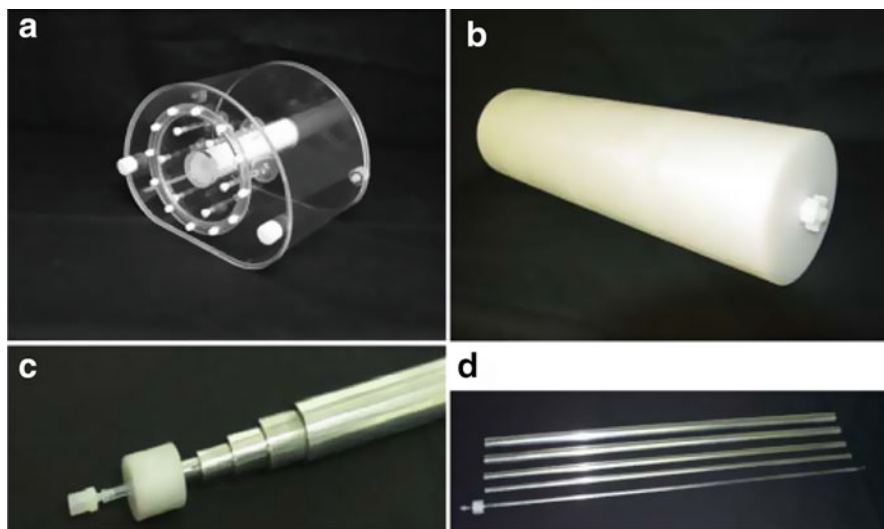


**Fig. 6.4** NEMA phantoms for PET performance tests. **(a)** This NEMA body phantom is used for evaluation of the quality of reconstructed images and simulation of whole-body imaging using camera-based coincidence imaging technique. **(b)** This phantom is used for measuring scatter fraction, dead time, and random counts in PET studies using the NEMA NU 2-2007 standard, **(c)** closeup end of the sensitivity phantom, **(d)** set of six concentric aluminum tubes used in phantom **(c)** to measure the sensitivity of PET scanners (Courtesy of Data Spectrum Corporation, Hillborough, NC)

tests in some scanners, and a new NU 2-2001 standard has been published by NEMA in 2001 (NEMA 2001) and corresponding new phantoms have been introduced.

Currently most PET scanners use the LSO or LYSO detectors composed of natural lutetium (Lu) that has a 2.6% radioisotopic content of  $^{176}\text{Lu}$  ( $t_{1/2} = 4.0 \times 10^{10}$  years). This isotope emits  $\beta^-$  particle and a cascade of high-energy  $\gamma$ - and X-rays. These intrinsic radiations cause errors in the performance parameters of a scanner such as the sensitivity, count losses, random events, etc. To correct for the contribution of this intrinsic activity, Watson et al. (2004) have recommended modifications in the performance tests and accordingly, NEMA has introduced the NEMA NU 2-2007 (2007) standard for these tests of PET scanners with Lu-based detectors. Many features of this standard have been kept the same as those of the NU 2-2001 standard, with some modifications for the sensitivity, count losses, and random events.

NEMA has recently published NU 2-2012 (2012) with minor changes to the 2007 version to make the tests reproducible and easy to carry out. No publication using this model for validation of commercial PET scanners has been reported in the literature as of this writing. Daube-Witherspoon et al. (2002) reported the methods of performing these tests based on the NEMA NU 2-2001 standard. The following is a brief description of these tests based on this article and the article of

Watson et al., and NEMA NU 2-2007, and NEMA NU 2-2012 standard has been alluded to, wherever needed. Refer to these publications for further details.

### Spatial Resolution

The spatial resolution of a PET scanner is determined by the FWHM of PSFs obtained from measurement of activity distribution from a point source. The spatial resolution can be transverse radial, transverse tangential, and axial, and these values are given in Table 6.1 for scanners from different manufacturers.

The spatial resolution is measured by using six-point sources of  $^{18}\text{F}$  activity contained in glass capillary in a small volume of less than  $1\text{ cm}^3$  (Daube-Witherspoon et al. 2002). *NEMA NU 2-2012 suggests an activity source contained in a capillary of 1 mm inner diameter and 2 mm length.* For axial resolutions, two positions—at the center of the axial FOV and at one-fourth of axial FOV from the center—are chosen (Fig. 6.5), whereas *NEMA NU 2-2012 suggests the latter position at three-eighth of the axial FOV from the center.* At each axial position, three point sources are placed at  $x=0, y=1\text{ cm}$  (to avoid too many sampling of LORs);  $x=10, y=0\text{ cm}$ ; and  $x=0, y=10\text{ cm}$ . Data are collected for all six positions and from reconstructed image data, PSFs are obtained in X, Y, and Z directions for each point source at each axial position. The FWHMs are determined from the width at 50% of the peak of each PSF, totaling 18 in number.

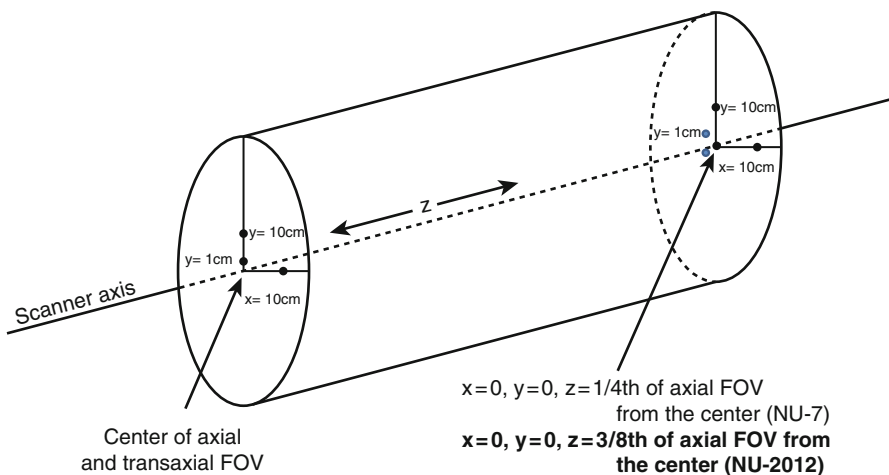


**Fig. 6.5** Arrangement of six-point sources in the measurement of spatial resolution. Three sources are positioned at the center of the axial FOV and three sources are positioned at one-fourth of the axial FOV (NEMA 7) or three-eighth of the axial FOV (NEMA 12) away from the center. At each position, sources are placed on the positions indicated in a transverse plane perpendicular to the scanner axis (Reprinted with the permission of the Cleveland Clinic Center for Medical Art and Photography ©2009. All rights reserved)

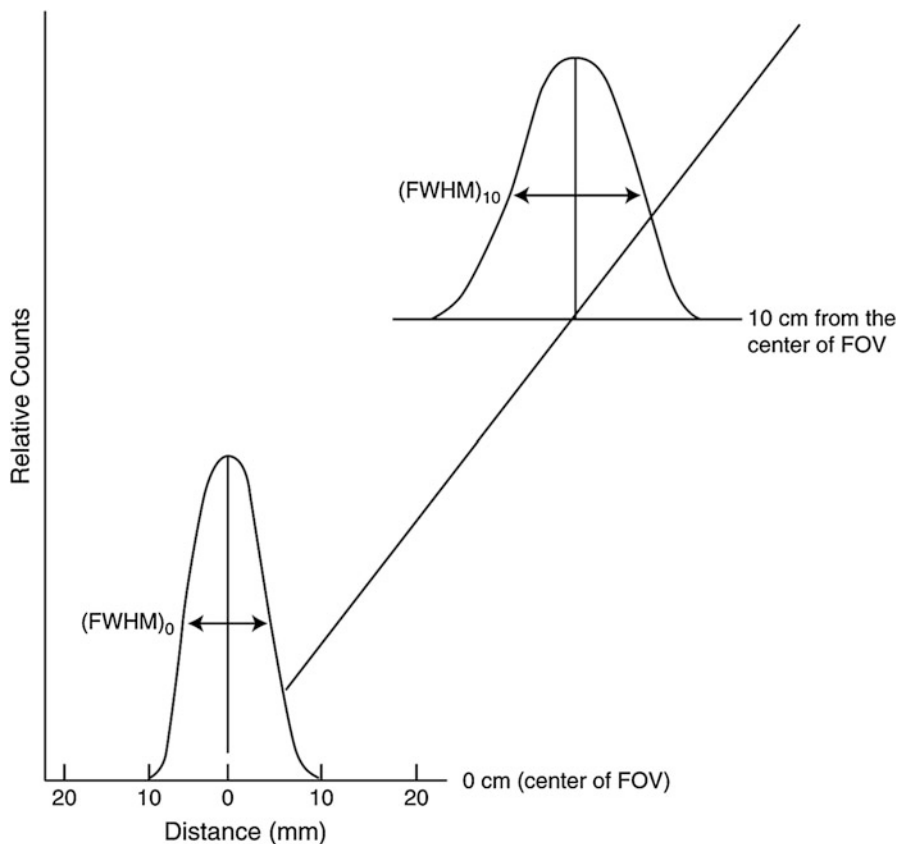


**Fig. 6.6** Point-spread functions (PSF) at 0 and 10 cm from the FOV. The transverse resolution (FWHM) is best at the center and worsens radially across the FOV (Reprinted with the permission of the Cleveland Clinic Center for Medical Art and Photography ©2009. All rights reserved)

Related FWHMs are combined and then averaged for the two axial positions to give the transverse radial, transverse tangential, and axial resolutions. Transverse resolution worsens as the source is moved away from the center of the FOV (Fig. 6.6), i.e., the resolution is best at the center and deteriorates toward the periphery of the scanner.

### ***Scatter Fraction***

Scattered radiations add noise to the reconstructed image, and the contribution varies with different PET scanners. Normally the test is performed with a very high activity source counted over a period of time, from which high activity data are used for determination of random events and count losses (see later) and low activity



data for scatter fraction. A narrow line source made of 70-cm-long plastic tubing and filled with high activity of  $^{18}\text{F}$  is inserted into a  $70 \times 20$ -cm cylindrical polyethylene phantom through an axial hole made at a radial distance of 4.5 cm and parallel to the central axis of the phantom (Fig. 6.4b). NEMA NU 2-2012 recommends similar parameters for the test. The phantom is placed at the center both axially and radially on the scan table such that the source is closest to the patient table, since the line source and the bed position affect the measured results.

Data acquisition is recommended in two ways based on whether random events are estimated separately for scanners with Lu-based detectors or they are assumed negligible as in scanners with non-Lu detectors. If the random events are to be estimated independently for Lu-based scanners, then data are acquired over time using two windows—a peak window and a delayed window—until both dead-time count losses and random events are reduced to less than 1% of the true rates. For PET scanners with non-Lu detectors, data acquisition is continued with only a peak window until the random-to-true ratio is less than 1% (NEMA 2007). The data are used to form both random and prompt sinograms, which are basically 2D representation of projection rays versus angle. Oblique projections are assigned to the slice where they cross the scanner axis using single-slice rebinning. The sinogram profile of an extended diameter of 24 cm (4 cm larger than the phantom) is generated, because the FOV varies with different scanners. Each projection in the sinogram is shifted so that the peak of the projection is aligned with the center of the sinogram (line source image). This produces a sum projection with a count density distribution around the maximum counts (peak) at the center of the sinogram (NEMA 2001, 2007). It is arbitrarily assumed that all true events including some scatter lie within a 4-cm-wide strip centered in each sinogram of the line source and that there are no true events but scatter events beyond  $\pm 2$  cm from the center of the sinogram. Thus, the total count  $C_T$  is the area under the peak in prompt sinogram that includes true events plus scatter and random events. In the case of PET scanners with non-Lu detectors,  $C_T$  will contain only the true plus scatter events.

For Lu-based PET scanners, random counts are estimated from the delayed window sinograms for all projections in a slice to give  $C_R$  for the slice, which is then applied to calculate true and scatter events. For non-Lu scanners, random events are negligible and not measured separately.

Scattered events under the peak are estimated by taking the average of the pixel counts at  $\pm 2$ -cm positions from the center, multiplying the average by the number of pixels (obtained by interpolation) along the 4-cm strip and finally adding the product to the counts in pixels outside the strip. This gives total scatter events ( $C_S$ ) for the slice. Using the values of  $C_T$ ,  $C_R$ , and  $C_S$ , the true count for a slice is calculated as

$$C_{\text{true}} = C_T - C_R - C_S \quad (6.9)$$

and for PET scanners with non-Lu detectors, the true count is

$$C_{\text{true}} = C_{\text{T}} - C_{\text{S}}. \quad (6.10)$$

The scatter fraction  $SF_i$  for the slice is given by Eq. (6.5) as

$$SF_i = C_{\text{S}} / (C_{\text{true}} + C_{\text{S}}). \quad (6.11)$$

The system scatter fraction SF is calculated from the weighted average of the  $SF_i$  values of all slices. These values are given in Table 6.1 for several PET scanners.

Note that counting rates for each component are calculated by dividing the respective counts by time of acquisition to give total count rate  $R_{\text{T}}$ , true count rate  $R_{\text{True}}$ , random count rate  $R_{\text{R}}$ , and scatter count rate  $R_{\text{S}}$ .

### Sensitivity

Sensitivity is a measure of counting efficiency of a PET scanner and is expressed in count rate (normally, cps) per unit activity concentration (normally, MBq or  $\mu\text{Ci}$  per cc).

According to NEMA NU 2-2001 and NEMA NU 2-2007 standards, a 70-cm-long plastic tube filled with a known amount ( $A_{\text{cal}}$ ) of a radionuclide is used (Fig. 6.4c, d) (Daube-Witherspoon et al. 2002). The level of activity is kept low so as to have random rate less than 5% of the true counts and count loss less than 1% (<5% according to NEMA NU 2-2012). The source is encased in metal sleeves of various thicknesses and suspended at the center of the transverse FOV in parallel to the axis of the scanner in such a way that the supporting unit stays outside the FOV.

Successive data are collected in sinograms using five metal sleeves. Duration of acquisition and total counts in the slice are recorded for each sleeve, from which the count rate is calculated. Count rates are corrected for decay to the time of calibration of radioactivity and then summed for all slices to give the total count rate for each sleeve. Next, the natural logarithm of the measured total count rate ( $R_{\text{T}}$ ) is plotted as function of sleeve thicknesses. After fitting of the data by linear regression, the extrapolated count rate ( $R_0$ ) with no metal sleeve (no attenuation) is obtained. For non-Lu scanners, the random rate ( $R_{\text{R}} = C_{\text{R}}/T_{\text{acquisition}}$ ) is negligible. Scatter count rate determined by the method described previously is subtracted from  $R_0$  to give the true count rate ( $R_{\text{true}}$ ) for the system. Thus,

$$R_{\text{true}} = R_0 - R_{\text{S}}. \quad (6.12)$$

For Lu-based scanners, there is an intrinsic activity as well as possible intrinsic random events due to  $^{176}\text{Lu}$ , which need to be subtracted from the total count rate.

These can be measured with the plastic tubing in place in the scanner but without any activity in it. Both prompt and delayed acquisitions are made of the tubing as described in the section on Scatter Fraction, from which intrinsic prompt rate and intrinsic random rate are calculated. The true intrinsic count rate  $R_{\text{int}}$  is obtained by subtracting the random rate from the prompt rate in all sinograms. Thus, for Lu-based scanners, true count rate  $R_{\text{true}}$  is given as

$$R_{\text{true}} = R_0 - R_S - R_R - R_{\text{int}}. \quad (6.13)$$

The system sensitivity is calculated as

$$S = R_{\text{true}}/A_{\text{cal}}, \quad (6.14)$$

where  $A_{\text{cal}}$  is the calibrated activity added to the tubing. The sensitivity is given in either cps/ $\mu\text{Ci/cc}$  or cps/kBq/cc. The measurement of sensitivity is repeated with the source placed radially at 10 cm from the center of the transverse FOV. The system sensitivity of commercial PET scanners is given for both 0- and 10-cm positions and the values for some scanners at the center of FOV are given in Table 6.1.

### ***Count Rate Loss and Random Coincidence***

To characterize the count rate behavior of a PET scanner at high activity, random events, NECR, and dead-time loss are determined as a function of activity. The activity source is the same as described above under Scatter Fraction in this chapter. A high activity source of  $^{18}\text{F}$  is used to acquire the sinogram, and data are collected until the activity level is low enough to consider random events and dead-time count losses to be negligible. The total counts are obtained from each high activity sinogram, which comprise true, random, and scatter events. The total count rate  $R_T$  is obtained by dividing the total counts by the duration of acquisition. As in scatter fraction experiment, the low activity data are used to calculate the scatter fraction  $SF_i$  and the true count rate  $R_{\text{true}}$  for each slice Eqs. (6.9)–(6.11). The random count rate  $R_R$  at high activity acquisition for each slice is then calculated according to Daube-Witherspoon et al. (2002) as

$$R_R = R_T - [R_{\text{true}}/(1 - SF_i)]. \quad (6.15)$$

The system random count rate is calculated by summing  $R_R$  values for all slices.

The NECR for each slice is computed by Eq. (6.4) as

$$(\text{NECR}) = (R_{\text{true}})^2 / R_{\text{T}}. \quad (6.16)$$

The system NECR is computed as the sum of NECRs for all slices. These values for some PET scanners are shown in Table 6.1.

The percent dead-time count loss (%DT) as function of activity is calculated by

$$\%DT = (1 - R_{\text{true}}/R_{\text{extrap}}) \times 100, \quad (6.17)$$

where  $R_{\text{extrap}}$  is the count rate extrapolated from the low activity data to the activity at the time when the total count rate  $R_{\text{T}}$  is measured.

## Questions

1. The typical transaxial resolution at 1 cm of a PET scanner ranges between (a) 14 and 16 mm, (b) 3 and 4 cm, or (c) 4 and 7 mm.
2. What are the common factors that affect the spatial resolution of a PET scanner? Out of these, which one is most predominant?
3. The transverse resolution is worse at the center of the FOV than away from the center. True \_\_\_\_\_; False \_\_\_\_\_.
4. The axial resolution of a scanner is its ability to differentiate two points on an image along the axis of the scanner. True \_\_\_\_\_; False \_\_\_\_\_.
5. If the detector size is 8 mm, what is the expected approximate spatial resolution for  $^{18}\text{F}$ -FDG PET images at the center of the FOV?
6. The maximum positron energy for  $^{18}\text{F}$  is 0.64 MeV and for  $^{82}\text{Rb}$  is 3.35 MeV. Which radiopharmaceutical would provide better spatial resolution?
7. Noncolinearity is a factor that affects the spatial resolution of a PET scanner. How is it affected by the diameter of the detector ring? For a 90-cm diameter detector ring, what is the value of the noncolinearity component in the overall spatial resolution?
8. Describe the method of measuring transverse radial, transverse tangential, and axial spatial resolutions of a PET scanner.
9. Define the sensitivity of a PET scanner and discuss the important parameters that affect the sensitivity.
10. Scanner 1 has twice the ring diameter of scanner 2. The ratio of sensitivities of scanner 1 to scanner 2 is:
  - (a) 0.75
  - (b) 0.67
  - (c) 0.25

11. The sensitivity in 3D acquisition is four to eight times higher than in 2D acquisition. Why?
12. The overall sensitivities of PET scanners in 2D mode are:
  - (a) 1–2%
  - (b) 3–5%
  - (c) 0.2–0.5%and in 3D mode:
  - (a) 2–10%
  - (b) 0.5–1%
  - (c) 15–20%
13. Scanner 1 has the detectors of size 3 mm, and scanner 2 has the detectors of size 6 mm. Assuming that all detectors are squares and all other parameters are the same, the sensitivity of scanner 1 is: (a) half, (b) one-tenth, or (c) one-fourth of scanner 2.
14. Describe the methods of daily and weekly quality control tests for PET and CT scanners.
15. Explain why and how normalization of PET acquisition data is carried out.
16. What are acceptance tests? Describe the methods of determining sensitivity and scatter fraction for a PET scanner.
17. The NECR is proportional to the signal-to-noise ratio in the reconstructed image. True \_\_\_\_\_; False \_\_\_\_\_.
18. The sensitivity of a scanner increases with (a) the size of the detector in the ring True \_\_\_\_\_; False \_\_\_\_\_ and (b) with the diameter of the detector ring True \_\_\_\_\_; False \_\_\_\_\_.
19. Scanner 1 has the individual detector size of  $36 \text{ mm}^2$  and scanner 2 has the detector size of  $60 \text{ mm}^2$ . Scanner 1 has (a) 30%, (b) 60%, or (c) 1.7 times the sensitivity of scanner 2.
20. Define contrast of an image. Elucidate the different factors that affect the contrast.
21. Increasing administered activity increases the spatial resolution. True \_\_\_\_\_; False \_\_\_\_\_.
22. Increasing administered activity increases the contrast resolution. True \_\_\_\_\_; False \_\_\_\_\_.
23. The daily QC check of CT scanner includes (a) laser alignment, (b) CT number of water, (c) tomographic uniformity, or (d) tomographic image noise.
24. Define CTDI.
25. Elucidate different parameters that are measured in the quality control of MR scanner.
26. What type of phantoms are used in MR quality control tests.

## References and Suggested Reading

- AAPM. Report no 100. Acceptance testing and quality assurance procedures for magnetic resonance imaging facilities. 2010.
- Brix G, Zaers J, Adam LE, et al. Performance evaluation of a whole-body PET scanner using the NEMA protocol. *J Nucl Med.* 1997;38:1614.
- Buchert R, Bohuslavizki UH, Mester J, et al. Quality assurance in PET: evaluation of the clinical relevance of detector defects. *J Nucl Med.* 1999;40:1657.
- Budinger TF. PET instrumentation: what are the limits? *Semin Nucl Med.* 1998;28:247.
- Cherry SR, Sorensen JA, Phelps ME. *Physics in nuclear medicine.* 3rd ed. Philadelphia: Saunders; 2003.
- Daube-Witherspoon ME, Karp JS, Casey ME, et al. PET performance measurement using the NEMA NU 2-2001 standard. *J Nucl Med.* 2002;43:1398.
- Huesman RH. The effects of a finite number of projection angles and finite lateral sampling of projections on the propagation of statistical errors in transverse section reconstruction. *Phys Med Biol.* 1977;22:511.
- Karp JS, Daube-Witherspoon ME, Hoffman EJ, et al. Performance standards in positron emission tomography. *J Nucl Med.* 1991;32:2342.
- Kearfott K. Sinograms and diagnostic tools for the quality assurance of a positron emission tomograph. *J Nucl Med Technol.* 1989;17:83.
- Keim P. An overview of PET quality assurance procedures: part 1. *J Nucl Med Technol.* 1994;22:27.
- Moses WW, Derenzo SE. Empirical observation of performance degradation in positron emission tomographs utilizing block detectors. *J Nucl Med.* 1993;34:101P.
- National Electrical Manufacturers Association. NEMA Standards Publications NU 2-1994. Performance measurements of positron emission tomographs. Washington, DC: National Electrical Manufacturers Association; 1994.
- National Electrical Manufacturers Association. NEMA Standard Publication NU 2-2001. Performance measurements of positron emission tomographs. Rosslyn: National Electrical Manufacturers Association; 2001.
- National Electrical Manufacturers Association. NEMA Standard Publication NU 2-2007. Performance measurements of positron emission tomographs. Rosslyn: National Electrical Manufacturers Association; 2007.
- National Electrical Manufacturers Association. NEMA Standard Publication NU 2-2012. Performance measurements of positron emission tomographs. Rosslyn: National Electrical Manufacturers Association; 2012.
- Tarantola G, Zito F, Gerundini P. PET instrumentation and reconstruction algorithms in whole-body applications. *J Nucl Med.* 2003;44:756.
- Watson CC, Casey ME, Eriksson L, et al. NEMA NU2 performance tests for scanners with intrinsic activity. *J Nucl Med.* 2004;45:822.
- Zanzonico P. Routine quality control of clinical nuclear medicine instrumentation: a brief review. *J Nucl Med.* 2008;49:1114.